RSC Advances

PAPER

View Article Online
View Journal | View Issue



Cite this: *RSC Adv.*, 2020, **10**, 23002

# Parent and nano-encapsulated ytterbium(III) complex toward binding with biological macromolecules, *in vitro* cytotoxicity, cleavage and antimicrobial activity studies†

Zahra Aramesh-Boroujeni, *[ab] Shohreh Jahani, [c] Mozhgan Khorasani-Motlagh,[d] Kagan Kerman [e] and Meissam Noroozifar*[e]

To determine the chemotherapeutic and pharmacokinetic aspects of an ytterbium complex containing 2,9-dimethyl-1,10-phenanthroline ($Me_2Phen$), *in vitro* binding studies were carried out with FS-DNA/BSA by employing multiple biophysical methods and a molecular modeling study. There are different techniques including absorption spectroscopy, fluorescence spectroscopy, circular dichroism studies, viscosity experiments (only in the case of DNA), and competitive experiments used to determine the interaction mode between DNA/BSA and the ytterbium-complex. The results showed that the Yb-complex exhibited a high propensity for the interaction of BSA and DNA *via* hydrophobic interactions and van der Waals forces. Further, a competitive examination and docking study showed that the interaction site of the ytterbium complex on BSA is site III. The results of docking calculations for DNA/BSA were in good agreement with experimental findings. The complex displays efficient DNA cleavage in the presence of hydrogen peroxide. Moreover, antimicrobial studies of different bacteria and fungi indicated its promising antibacterial activity. *In vitro* cytotoxicity studies of the Yb-complex, starch nano-encapsulated, and lipid nano-encapsulated were carried out in MCF-7 and A-549 cell lines, which revealed significantly good activity. The results of anticancer activity studies showed that the cytotoxic activity of the Yb-complex was increased when encapsulated with nanocarriers. Based on biological applications of the Yb-complex, it can be concluded that this complex and its nanocarriers can act as novel anticancer and antimicrobial candidates.

Received 30th April 2020
Accepted 4th June 2020

DOI: 10.1039/d0ra03895d

rsc.li/rsc-advances



## 1. Introduction

Studies on the synthesis and antitumor properties, along with their reactivity towards protein and DNA, of small molecules are of recent importance in linking information about tools for molecular biology, metabolism and transporting procedure, and drug design. Therefore, several scientists today focus on the development of novel metal-based antitumor drugs with non-covalent binding modes that target DNA.[1,2] DNA is the target molecule for many medications, particularly anticancer drugs. The binding of metal complexes with DNA is the topic of interest in various study fields, for example, medicinal chemistry, cancer therapy, life science, biochemistry, *etc.*[3–6] The metal compounds used as antitumor factors can bind to carrier proteins in the blood. Albumins are the essential extracellular and the most abundant protein constituent of the vascular system. Both human serum albumin (HSA) with 585 amino acid residues, which has one Trp (Trp-214), and bovine serum albumin (BSA) with 583 amino acid residues, which has two Trp (Trp-134 and Trp-213), are types of globular and non-glycosylated protein. Their three-dimensional structure is like the shape of the heart and consists of three homologous domains and each domain comprises two subdomains (A and B).[7,8]

In this context, binding toward serum proteins that may perform a transport function for metal complexes appears to be the most important issue because such interactions determine also the overall drug distribution and excretion and differences in efficacy, activity, and toxicity.[8–11]

The coordination chemistry of lanthanides (Ln) has disclosed considerable development in several decades because of

[a]*Department of Clinical Laboratory, AlZahra Hospital, Isfahan University of Medical Sciences, Isfahan, Iran. E-mail: zaramesh.boroujeni@gmail.com*

[b]*Young Researchers and Elite Club, Najafabad Branch, Islamic Azad University, Najafabad, Isfahan, Iran*

[c]*Nano Bioeletrochemistry Research Center, Bam University of Medical Sciences, Bam, Iran*

[d]*Department of Chemistry, University of Sistan and Baluchestan, Zahedan 98135-674, Iran*

[e]*Department of Physical and Environmental Sciences, University of Toronto Scarborough, 1265 Military Trail, Toronto, Ontario, M1C 1A4, Canada. E-mail: m.noroozifar@utoronto.ca*

† Electronic supplementary information (ESI) available. See DOI: 10.1039/d0ra03895d

its various applications.[12] The $Ln^{3+}$ ions perform as hard Lewis acids. Hence, their junctions with hard molecules with oxygen donor atoms will be robust. The lanthanide compounds design is concentrated on potential applications in parts like separation, nonlinear optics, catalysis, magnetism, luminescent probes, and extraction, or is indicating in therapeutic potential as antibacterial, antifungal, anticancer, or antioxidant agents. Due to their lifetimes and long-wavelength fluorescence, lanthanide compounds have the potential for application as probes and sensors in the medical and biological studies.[13–17]

One of the best ways to improve the antitumor activity and reduce the side effects of metal complexes is their encapsulation into starch, lipid and liposome microspheres. Nanocapsules offer a broad range of interesting features over their micro-sized counterparts as they hold more surface area, have enhanced solubility, significantly higher biocompatibility, biodegradability, stability during storage, and controlled release.[18,19]

In continuation of our previous paper,[20–25] we decided to expose the luminescence of the Yb(III) containing $Me_2Phen$ ligand, $[Yb(Me_2Phen)_2Cl_3(OH_2)]$ and to introduce it as a novel probe to BSA (Bovine Serum Albumin) and FS-DNA (Fish-Salmon DNA). Thus, the binding of the ytterbium complex with BSA and FS-DNA was examined by emission spectroscopy, UV-vis titration, viscosity measurement, CD spectroscopy, and docking method. Also, the ability of this complex to cleave DNA by gel electrophoresis was reported. Moreover, nanocarriers of this complex produced, and the anticancer, antifungal, and antibacterial properties of this complex studied.

## 2. Experimental

### 2.1. Materials and apparatus

FS-DNA, BSA, and EtBr were obtained from Sigma-Aldrich. Tris(hydroxymethyl)-aminomethane (Tris–HCl) and other chemicals were purchased from Merck. All chemicals and solvents were used as received without further purification. The ytterbium-complex was prepared according to previously reported in our earlier work.[21]

Electronic absorption measurements were carried out using the Analytik Jena SPEC ORD S100 spectrometer at room temperature. Fluorescence experiments were performed on a PERKIN ELMER, LS-3 equipped with thermostat cell compartment which kept temperature constant within ±0.1 °C. Fluorescence titration carried out at different temperatures (290, 295, 298, 301, and 303 K). The widths of both the excitation and emission slits were set at 5.0 nm. Circular dichroism (CD) studies were done by an Aviv Circular Dichroism Spectrometer (model 215) at 298 K, and the viscosity experiment was performed by a viscometer (SCHOT AVS 450) at room temperature. Inductively coupled plasma (ICP) spectrometer was employed to determine the amount existing of ytterbium in the lipid nanoencapsulation (LNEP) and the starch nanoencapsulation (SNEP).

### 2.2. FS-DNA and BSA binding experiments

All the solutions were made in Tris–HCl buffer (including 50 mM sodium chloride and 5 mM Tris–HCl) at pH = 7.2. The concentrations of FS-DNA, BSA and EtBr solutions were obtained by UV-vis spectrometry ($\varepsilon_{260}$ = 6600 $M^{-1}$ $cm^{-1}$, $\varepsilon_{280}$ = 44 300 $M^{-1}$ $cm^{-1}$ and $\varepsilon_{480}$ = 5450 $M^{-1}$ $cm^{-1}$ for FS-DNA, BSA and EtBr, respectively[2,23]). Also, DNA purity was tested by the observance of the ratio of absorption at 260 and 280 nm. The solution of FS-DNA provided $A_{260}/A_{280}$ > 1.80, presenting that the deoxyribonucleic acid was satisfactorily free from protein pollution.[26] All the solutions were kept at four degrees centigrade and consumed after no more than four days. The stability of the ytterbium(III) complex was tested in aqueous solution through the UV-vis spectra of the Yb-compound several times.

The Yb-complex has the fluorescence in 300–450 nm at $\lambda_{ex}$ = 270 nm (the excitation wavelength), but quantum efficiencies of complex were much lower than protein. However, the intensity fluorescence of the Yb-complex is much lesser than the protein solution in the concentration range of this work. Thereby, emission spectra measurements were modified by considering of these values that is negligible. The inner filter effect (IFE) was considered in the emission titration data. Usually, the emission intensity with IFE can be modified using eqn (1):[1,8,27]

$$F_{cor} = F_{obs} \times 10^{\frac{A_1+A_2}{2}} \quad (1)$$

where $F_{obs}$ and $F_{cor}$ are the observed emission intensity and the corrected emission intensity, respectively. $A_1$ and $A_2$ are the total absorptions of all components at $\lambda_{ex}$ and $\lambda_{em}$, respectively.

### 2.3. Molecular docking

From the Brookhaven protein data bank, the crystal structures of DNA duplex (entry codes 1BNA and with sequence $d(CGCGAATTCGCG)_2$ dodecamer) and BSA (entry codes 3v03) were downloaded. Forgiving the most stable geometric of the ytterbium complex, the structure optimizing calculation was performed by Gaussian 09 at the 6–31 G** level by using the B3LYP hybrid density functional theory (DFT).[28] Autodock4.2.6 was applied by a semi-flexible docking technique. In this study, all the Yb-complex bonds were set free while BSA and DNA kept rigid. Also, the different regions of BSA selected for the docking (three BSA active sites). The gridpoint spacing of 0.375 Å and the grid map with 70 Å × 70 Å × 70 Å points were created. The docking included the maximum 25 000 000 energy calculations, and 200 separate docking runs were performed utilizing the Lamarckian genetic algorithm local search technique.[29]

### 2.4. DNA cleavage experiments

The ytterbium complex ability for DNA cleavage can be examined by gel electrophoresis. In the presence and absence of hydrogen peroxide ($2.0 \times 10^{-4}$ M) as the oxidant, FS-DNA (1.4 mM) was added to Yb-complex solutions with the various amounts (1.2, 2.5, 3.7, and 5 mM) and then solution mixed. The solutions were incubated for 0.5 h at 25 °C. The solutions were quenched by addition of a loading buffer (30% glycerol (3 μL) + 0.25% xylene cyanol + 25% bromophenol blue). Then, electrophoresis was completed by at 50 V for 60 min in TAE buffer at pH = 7.2 (40 mM acetic acid, 1 mM EDTA, and 40 mM Tris-base) on an agarose gel. The agarose gel was stained for 20 min by keeping it in the EtBr solution (1 μg $cm^{-3}$). Then, it was de-

stained for 20 min by immersing in sterile distilled water. The bands were imagined by watching the gel by UV illumination and photographed.

### 2.5. Evaluation of cytotoxicity (MTT assay)

The LNEP and SNEP of the Yb complex were synthesized according to the literature.[19] The MTT examination studied the anticancer properties of the ytterbium complex, LNEP, and SNEP on A-549 and MCF-7 cell lines. The cell lines of A-549 and MCF-7 were incubated for one day at 37 °C in a humidified 5% $CO_2$, in the existence of the various amount of the Yb complex, SNEP, and LNEP. After this step, the solution of MTT (10 μL, 12 mM) was added, and then the plates were incubated for four hours. The culture media was rejected. After the addition of DMSO (50 μL), the wells were washed with phosphate-buffered saline and incubated for ten minutes. $IC_{50}$ is the 50% inhibition concentration which calculated at 545 nm by ELISA reader through the following eqn (2):[4]

$$\%\,\text{cell cytotoxicity} = [1 - (\text{drug absorption/control absorption})] \times 100 \quad (2)$$

For evaluating the influence of SNEP and LNEP on the anticancer properties, the cellular penetration examination was performed. The A-549 and MCF-7 cell lines with the cell culture (100 μL) medium including 0.15 μg Yb complex (130 μM), 1.29 μg SNEP or 1.15 μg LNEP (equivalent to 0.15 μg Yb complex) were incubated for one day in 5% $CO_2$ incubator. Afterward eliminating the supernatant, this mixes (the cells having Yb-complex) were treated with $CHCl_3$ and $HNO_3$. All studies were done three times.

### 2.6. Antibacterial test

The zone of inhibition testing, the plate-counting technique, the minimum inhibitory concentration (MIC), and the inoculation time examined the antibacterial activity of Yb-complex on five Gram-negative bacteria (*Acinetobacter baumannii* (*A. baumannii*), *Klebsiella pneumoniae* (*K. pneumoniae*, ATCC 10031), *Salmonella typhi* (*S. typhi*, ATCC 1609), *Pseudomonas aeruginosa* (*P. aeruginosa*, ATCC 27853), *Escherichia coli* (*E. coli*, ATCC 25922)) and four Gram-positive bacteria (*Enterococcus faecalis* (*E. faecalis*, ATCC 29212), Methicillin-resistant *Staphylococcus aureus* (*MRSA*), *Enterococcus faecium* (*E. faecium*), Vancomycin-resistant *Enterococcus* (*VRE*)) and one fungus *Candida albicans* (*C. albicans*).

In the inhibition zone diameter method, a stock inoculum with 700 CFU $mL^{-1}$ for dyes on the agar plate of Muller Hinton (MH) was applied. Afterward, discs of filter paper saturated with the antimicrobial matter (Yb-complex, 5 mg $mL^{-1}$) were transported on the plate. For taking the zone of inhibition, the incubation was carried out for one day at room temperature. The broth dilution technique did the plate-counting methods and MIC. Tubes, including MH broth, 5.0 mL, with ten-fold dilutions of antimicrobial agents (0.005–50 mg $L^{-1}$), were inseminated with 700 CFU $mL^{-1}$ of fungi and bacteria. Also, tubes were incubated for one day at 37 degrees centigrade; then, without shaking for visible turbidity, incubation tubes were studied. The minimum inhibitory concentration was found as the bottom dilution of this compound that made no noticeable turbidity.

After MIC have been detected, $1.0 \times 10^2$ L of inoculum from the content of the tube, without visible turbidity was subculture onto the agar plate and also incubated for one day. Then, the number of grown colonies on the subculture was contrasted to the number of CFU $mL^{-1}$ in the initial inoculum. The minimum bactericidal concentration (MBC) was referred to as the lowermost dilution of ytterbium compound allowed less than 0.1% of the initial inoculum to live. These studies were performed three times.

## 3. Results and discussion

### 3.1. The f–f transition of ytterbium complex

The Yb-complex revealed broadband at 372 nm ascribed to fluorescence $Me_2Phen$ ligand and luminescence characteristic of $Yb^{3+}$ with apparent bands in the region of 400–700 nm (Fig. 1(A)). As we can see in the figure, the f–f transitions for the Yb-complex presented four luminescence peaks at 633, 609, 545, and 495 nm, corresponding to $0' \rightarrow 3$, $0' \rightarrow 2$, $0' \rightarrow 1$, and $0' \rightarrow 0$ ($^2F_{5/2} \rightarrow {}^2F_{7/2}$) transition of $Yb^{3+}$ ion, respectively.[30]

The luminescence spectrum of the trivalent ytterbium cation definite that the $Me_2Phen$ was an excellent chelating chromophore and could be applied to absorb and transfer energy to $Yb^{3+}$ atom. Instead, the presentation of the ligand-centered luminescence peak at 372 nm indicated that the effective energy transfer from $Me_2Phen$ to the $Yb^{3+}$ center did not happen and energy transfer from $Yb^{3+}$ cation overcame.[31]

### 3.2. FS-DNA binding examinations

**3.2.1. Fluorescence measurements.** The emission experiment, a rapid and sensitive spectroscopic method, has been

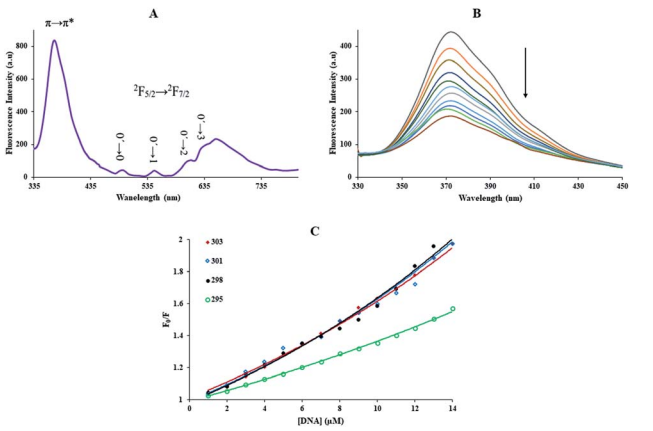


Fig. 1 (A) Fluorescence spectrum of Yb-complex (1.0 mM), at 298 K, $\lambda_{ex}$ = 300 nm, in $CH_3CN$ solution. (B) Fluorescence spectra of Yb complex in the presence and absence of different FS-DNA concentrations, $\lambda_{ex}$ = 270 nm, [DNA] = 0 to 14.3 μM and [complex] = 0.1 μM, (C) the Stern–Volmer plots of the fluorescence quenching of complex induced by FS-DNA at the different temperatures.

 

Table 1 The binding constant ($K_b$), the number of the binding sites ($n$), the biomolecular quenching rate constant $k_q$, the Stern–Volmer constant ($K_{SV}$), and thermodynamic parameters ($\Delta S^\circ$, $\Delta H^\circ$, and $\Delta G^\circ$) for the interaction of DNA with ytterbium complex at various temperatures

| | | | $K_b \times 10^{-5}$ ($M^{-1}$) | | | | | |
|---|---|---|---|---|---|---|---|---|
| $T$ (K) | $k_q \times 10^{-12}$ ($M^{-1}$ $s^{-1}$) | $K_{SV} \times 10^{-4}$ ($M^{-1}$) | UV | Fluorescence | $n$ | $\Delta S^\circ$ (J $mol^{-1}$ $K^{-1}$) | $\Delta H^\circ$ (kJ $mol^{-1}$) | $\Delta G^\circ$ (kJ $mol^{-1}$) |
| 290 | 3.18 ± 0.04 | 3.18 ± 0.04 | | 0.64 ± 0.02 | 1.00 | | | −26.70 ± 0.04 |
| 295 | 3.27 ± 0.04 | 3.27 ± 0.04 | | 1.62 ± 0.03 | 1.13 | | | −29.42 ± 0.03 |
| 298 | 5.58 ± 0.03 | 5.58 ± 0.03 | 1.49 ± 0.02 | 2.95 ± 0.05 | 1.13 | 528.80 ± 0.06 | 126.59 ± 0.04 | −31.20 ± 0.03 |
| 301 | 5.66 ± 0.04 | 5.66 ± 0.04 | | 4.07 ± 0.04 | 1.16 | | | −32.32 ± 0.06 |
| 303 | 6.25 ± 0.05 | 6.25 ± 0.05 | | 6.45 ± 0.05 | 1.19 | | | −33.70 ± 0.05 |

usually applied to investigate the bindings between metal complexes and macromolecules.[32] The investigating of DNA interaction is the primary step to the pharmacological goal of anticancer examine, and therefore considerate the DNA-interaction mechanism is more significant.[1] For compounds with luminescence properties, emission experiment is the perfect study technique, which measures the difference in emission intensity after and before the interaction.[32] Fig. 1(B) showed the emission spectra of the ytterbium complex (0.1 μM) with various amounts of FS-DNA (0–14.3 μM). The Yb-complex exhibited the fluorescence band at 372 nm ($\lambda_{ex}$ = 270 nm). The complex exhibited emission quenching with enhancing concentrations of FS-DNA. The results show that FS-DNA could quench the complex emission and that interaction of DNA to Yb-complex indeed happens.

The emission quenching technique further investigated the binding of the Yb-complex and DNA. The emission quenching happens by various mechanisms, which are generally classified as dynamic and static. Static quenching exhibits to formation complex of quencher–fluorophore (FS-DNA–Yb-complex). Still, dynamic quenching mentions to a procedure in which the quencher (FS-DNA) and the excited fluorophore (Yb-complex) requires contact.

With growing temperature, it is possible the results of the reduction in the stability of the complex, and so quenching constants values ($K_{SV}$) were decreased. But, dynamic quenching depends upon diffusion, and since higher temperatures result in more significant diffusion coefficients, $K_{SV}$ values were exaggerated by raising the temperature.[33,34] The only dynamic or static quenching procedure can cause a linear plot $F_0/F$ *vs.* [Q] (eqn (3)), and based on the classical theory of emission quenching; a nonlinear plot can be the combination of quenching type.[32]

$$\frac{F_0}{F} = 1 + K_{SV}[Q] = 1 + k_q\tau[Q] \quad (3)$$

where $F$ and $F_0$ are the emission intensities in the presence and the absence of FS-DNA (quencher), respectively. The $\tau_0$ is the average biomolecule lifetime without quencher ($\tau_0 = 10^{-8}$ s (ref. 35)), $k_q$ is the fluorophore quenching rate constant, and [Q] is the quencher concentration (FS-DNA). For static quenching, the dependence of the fluorescence intensity upon quencher concentration is easily derived by consideration of association constant ($K_S$) for complex formation and described by the following equation:[36]

$$\frac{F_0}{F} = 1 + K_S[Q] \quad (4)$$

Obviously, the dependence of $F_0/F$ on [Q] is linear for dynamic quenching and static quenching. However, for the combined dynamic and static quenching, the characteristic feature of the dependence of $F_0/F$ on [Q] is an upward curvature, concave towards the $Y$-axis. And the dependence of $F_0/F$ on [Q] is described by the following modified Stern–Volmer equation:[36]

$$\frac{F_0}{F} = (1 + K_S[Q])(1 + K_D[Q]) = 1 + (K_S + K_D)[Q] + K_SK_D[Q]^2 \quad (5)$$

where $K_S$ and $K_D$ are the static and dynamic quenching constants, respectively. From Fig. 1(C), the dependence of $F_0/F$ on [Q] is nonlinear in the concentration range of FS-DNA from 1.0 to 14.3 μM, indicating that the quenching mechanism of Yb-complex induced by FS-DNA may be the combined dynamic and static quenching. Meanwhile, it can be observed that the dependence of $F_0/F$ on [Q] is closely linear when the concentration of FS-DNA is lower than 7.00 μM, which is treated according to the Stern–Volmer equation and the results are listed in Table 1. The corresponding Stern–Volmer plots at 290, 298, and 303 K are shown in Fig. 2(A) and at 295 and 301 K are shown in Fig. S1(A)† (this was done for avoiding any ambiguity and better presentation of data). From Table 1, it can be found that the $K_{SV}$ increased with increasing temperature, suggesting that the quenching process is initiated by dynamic quenching. What's more, we observed that the values for $k_q$ are greater than the maximum diffusion collision quenching rate constant ($2.0 \times 10^{10}$ $M^{-1}$ $s^{-1}$),[7,36] indicating that the static quenching effect may exist in the system of Yb-complex and DNA. That is to say, the quenching mechanism of Yb-complex by FS-DNA is initiated by a combined quenching process (including dynamic and static quenching).

$K_b$ and the number of binding sites ($n$) for interaction DNA with the Yb-complex were analysed by eqn (6) using the data obtained from fluorescence titration:[6]

$$\log\frac{F_0 - F}{F} = \log K_b + n\log[Q] \quad (6)$$

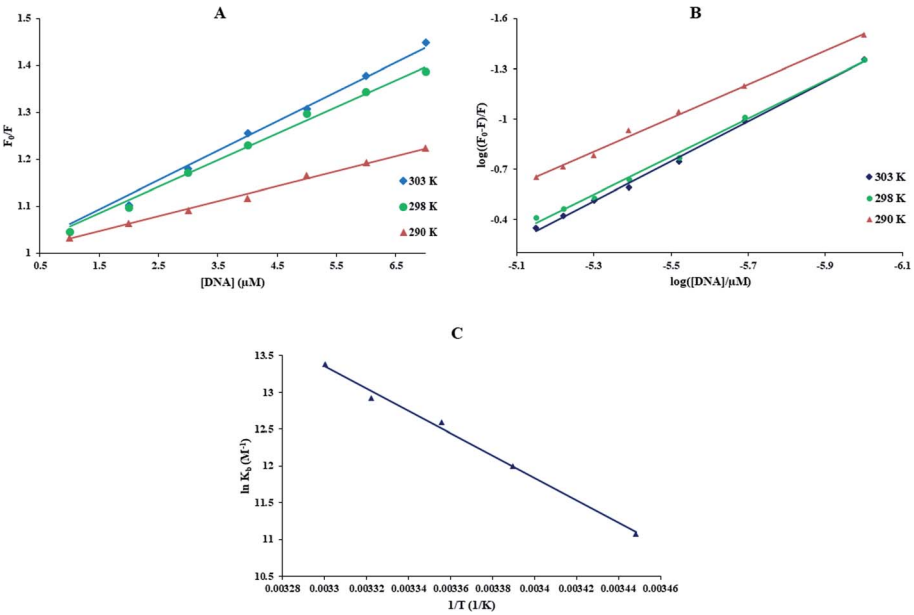


Fig. 2 (A) The $F_0/F$ *vs.* [DNA] curves, (B) the plot of log(($F_0 - F$)/$F$) *against* log([FS-DNA]/μM) at the different temperatures, (C) van't Hoff plot for the interaction of DNA with this complex $\lambda_{ex}$ = 270 nm, [DNA] = 0 to 14.3 μM and [complex] = 0.1 μM.

$K_b$ and $n$ were gotten at different temperatures (Table 1). The linear equations at 290, 298, and 303 K are shown in Fig. 2(B) (the relevant plots at 295 and 301 K are shown in Fig. S1(B)†). The $K_b$ value at 298 K is 2.95 ± 0.05 × $10^5$ $M^{-1}$ that indicating the high affinity of FS-DNA to Yb-complex, and the amount of $n$ is near to 1 exhibited that there is just a binding site for DNA with the Yb-complex.

**3.2.2. Thermodynamic studies.** The entropy ($\Delta S^\circ$), enthalpy ($\Delta H^\circ$) and free energy change ($\Delta G^\circ$) were obtained by the van't Hoff equation (eqn (7) and (8)) by the plotting of ln $K_b$ against 1/$T$ (Fig. 2(C)).[33]

$$\ln K_b = -\frac{\Delta G^\circ}{RT} = -\frac{\Delta H^\circ}{R}\left(\frac{1}{T}\right) + \frac{\Delta S^\circ}{R} \quad (7)$$

$$\Delta G^\circ = \Delta H^\circ - T\Delta S^\circ \quad (8)$$

The thermodynamic parameters of the Yb-complex were listed in Table 1. The model of binding between macromolecular and the complex can be concluded using by the thermodynamic parameters: (1) $\Delta H^\circ < 0$ and $\Delta S^\circ < 0$, hydrogen bonds and van der Waals interaction; (2) $\Delta H^\circ$ close to 0 and $\Delta S^\circ > 0$, electrostatic interactions; (3) $\Delta H^\circ > 0$ and $\Delta S^\circ > 0$, hydrophobic forces.[33,34] As Table 1 showed that the positive values of $\Delta S^\circ$ and $\Delta H^\circ$ revealed that hydrophobic forces play main roles in the interaction of FS-DNA to the Yb-complex. Also, the negative $\Delta G^\circ$ sign exposed to the DNA-binding procedure was spontaneous.

**3.2.3. Competition experiment by EtBr and rhodamine B.** It is well known that the binding mode of rhodamine B and EtBr with DNA are groove binding and intercalation, respectively. Rhodamine B and EtBr are commonly applied as luminescence analyses to investigate the interaction mode of compounds with DNA.[37–39] The effect Yb-complex addition on the fluorescence intensity of the DNA-EtBr mixture (70 μM and 3.0 μM, respectively) was studied (Fig. 3(A)). The emission intensity of EtBr enhanced significantly when it intercalates into DNA. Similar EtBr, if the compound intercalates with DNA, it leads to decreases in the DNA interaction sites that available for EtBr, which successively signifies decreases the fluorescence intensity of the EtBr-DNA mixture. As seen from this figure, the EtBr–DNA complex showed a fluorescence band at 587 nm by $\lambda_{ex}$ = 525 nm. A litter reduction in the luminesce intensity of the DNA-EtBr solution was detected during the adding of the Yb-complex. From insert Fig. 3(A), it is seen that at the end of the titration, the decrease in the emission intensity is only 12.1%. This data suggested that the interaction of FS-DNA with the Yb-complex was not similar to EtBr.

The rhodamine B binds to DNA by the groove binding, and it is used to research competitive replacement by groove binders. The fluorescence spectra rhodamine B-FS-DNA solution (3.0 μM and 70 μM, respectively) in the presence and absence of Yb-

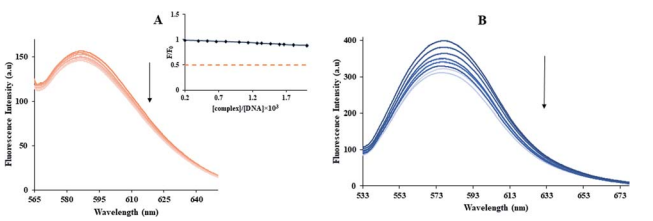


Fig. 3 (A) Fluorescence quenching curves of EtBr bound to DNA by Yb(III) complex ([DNA] = 70 μM, [EtBr] = 3.0 μM, [complex] = 0–145.7 μM). Inset is the plot of $F/F_0$ *vs.* ([complex]/[DNA]). (B) Fluorescence emission spectra of the mixture solutions of FS-DNA and rhodamine B in the presence of Yb-complex ([Rhodamine B] = 3.0 μM, [complex] = 0–145.7 μM, [FS-DNA] = 70 μM and $\lambda_{ex}$ = 520).

complex (0–145.7 μM) were investigated (Fig. 3(B)). In addition to the Yb-complex to the rhodamine B-FS-DNA, a remarkable reduction in the emission intensity of the rhodamine B-DNA was detected. This result showed that the ytterbium complex was able to replace rhodamine B. The results indicated that the Yb-complex bonds with FS-DNA with the groove binding rather than an intercalation binding.

**3.2.4. Effect of ionic strength.** To identify the interaction mode between FS-DNA and the Yb-complex, examine the ionic strength effect is a useful technique. The electrostatic binding happens from outside of the DNA strand, but the non-intercalative and intercalative binding intimately are bond to the DNA helix. When the DNA – the compound system was titrated by sodium chloride, because of electrostatic interaction, the compound was released from the DNA-compound system and resulted in an increased in the fluorescence intensity. The influence of sodium chloride on the emission of the Yb complex in the existence of FS-DNA (4.4 μM) was examined (Fig. S2†). The data presented that with the adding of sodium chloride (0.05 to 0.6 M) to the Yb-complex-DNA solution, no considerable change in the emission intensity has happened, which proposes that a non-electrostatic interaction of DNA to Yb complex.

**3.2.5. KI quenching experiments.** The emission quenching of Yb-complex (0.1 μM) by anionic quencher KI (4.0–40.0 mM) in the presence and absence of FS-DNA (4.4 μM) was examined for determining the interaction mode of Yb-complex with FS-DNA. The negative charge of $I^-$ can effectively quench the Yb-complex emission. As is well known, FS-DNA holds a negative charge of phosphate anchor, hence the $I^-$ is readily repulsed by it. Therefore the fluorescence intensity is well protected of the intercalating compounds from being quenched.[40]

But, non-intercalative binding provides a little protection for the fluorophore as the fluorophore is revealed to the surroundings, and $I^-$ can immediately quench its emission even in the FS-DNA attendance.[40] Using eqn (3) availability of Yb-complex to $I^-$ in the presence and absence of DNA was investigated (Fig. 4(A)), and the values of $K_{SV}$ were determined. As seen in insert of Fig. 4(A), $I^-$ quenched the Yb complex emission in the presence ($K_{SV} = 23.32\ M^{-1}$) and the absence of FS-DNA (37.26 $M^{-1}$). These data propose that FS-DNA interacts with the Yb complex through the groove interaction.

**3.2.6. CD studies.** The circular dichroism experiment is a useful method in distinguish changes in DNA morphology in interacting DNA with compounds.[5] The CD spectrum of FS-DNA includes the peak at 282 nm and another peak at 238 nm owing to base stacking and right-handed helicity, respectively, that are quite sensitive to the binding kinds of compounds with DNA.[33]

The influence of the Yb-complex on the FS-DNA conformation as showed Fig. 4(B). As can be seen that with adding of the ytterbium complex to DNA solution, the decrease of both the positive and negative band intensity (shifting to zero levels) without the shift in $\lambda_{max}$ was indicated. This result revealed that the right-handed B form of FS-DNA is stabilized.[33] Therefore, these results are supported by a non-intercalative mode and suggest the groove mode.

**3.2.7. Viscosity measurements.** Viscosity experiments can found further evidence on the interaction mode of FS-DNA with the Yb complex. The partial interacting compounds and the groove binders usually occasion no change or less executed (negative or positive) in DNA viscosity. But, intercalating compounds are estimated to lengthen the double helix as inserting the compound in among the base pairs leading to an growth in the DNA viscosity.[33] The relative specific viscosity values of $(\eta/\eta_0)^{1/3}$ various [Yb-complex]/[FS-DNA] were plotted (Fig. S3†); where $\eta_0$, and $\eta$ are the DNA relative viscosities of in the absence and presence of Yb-complex, respectively. It can be seen that the Yb-complex causes an insignificant change in the viscosity of DNA, showing that Yb-complex interacts to DNA with the groove binding.

**3.2.8. UV-vis study.** UV-vis experiment is one of the most suitable methods in investigating of interaction compounds with DNA.[1] The absorption titration of Yb-complex (10 μM) in the absence and the presence of FS-DNA (1.1–11.1 μM) is given in Fig. 5(A). In general, the interaction between complexes and macromolecules through intercalation results in the bathochromic effect (hypochromic with a redshift). Moreover, the hyperchromic can be detected for the groove interaction between macromolecules and compounds, although the UV-vis

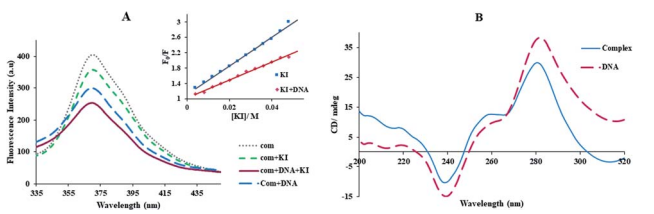


Fig. 4 (A) Fluorescence spectra of the Yb-complex with enhancing the KI concentration in the absence and presence of DNA, [KI] = 4.0–40.0 mM, [DNA] = 4.4 μM, and [complex] = 0.1 μM. Insert is the curves of Stern–Volmer of the emission titration data, (B) CD spectra of FS-DNA in the presence and absence the Yb complex, [complex] = $1.0 \times 10^{-5}$ M, [FS-DNA] = 5.9 mM.

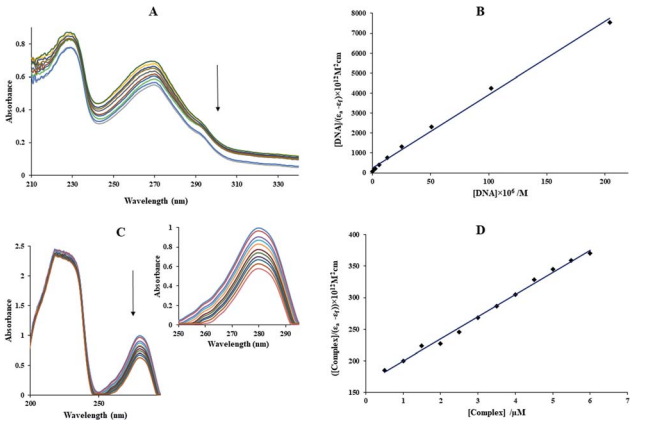


Fig. 5 (A) The UV-vis spectra of Yb complex in the presence and absence of different FS-DNA concentrations, [DNA] = 0–9.9 μM, [complex] = $1.0 \times 10^{-5}$ M, and $T = 25\ ^\circ C$. (B) The plot of [FS-DNA]/($\varepsilon_a - \varepsilon_f$) *against* [FS-DNA]. (C) The UV-vis spectra of BSA in the presence and absence of different Yb complex concentrations, [BSA] = $10 \times 10^{-6}$ M, [complex] = 0–$6.5 \times 10^{-6}$ M, $T = 25\ ^\circ C$. (D) The plot of [complex]/($\varepsilon_a - \varepsilon_f$) *against* [complex].

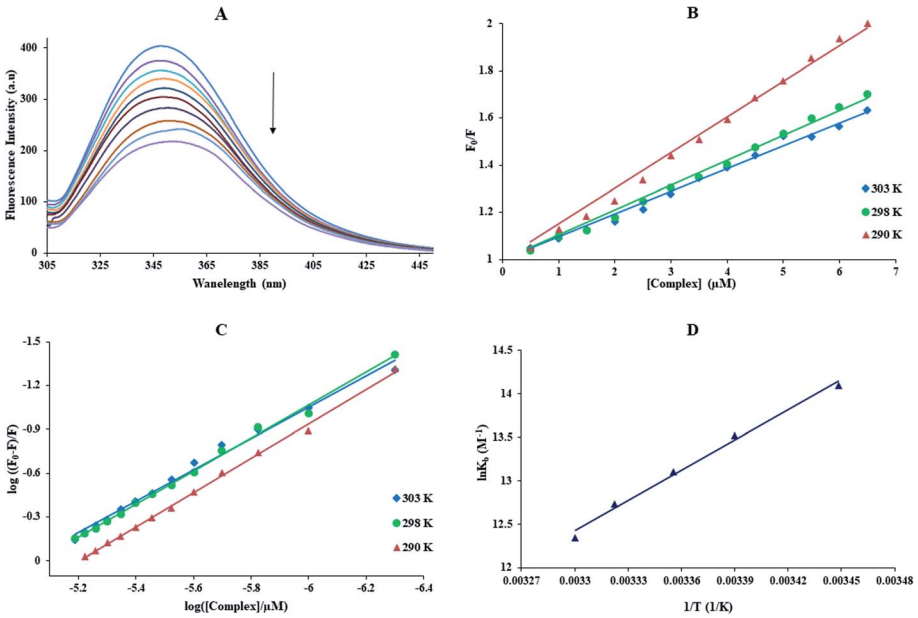


Fig. 6 (A) Fluorescence spectra of BSA in the presence and absence of different Yb complex concentrations, [complex] = 0–6.0 μM and [BSA] = 3 μM ($\lambda_{ex}$ = 280 nm and room temperature). (B) The $F_0/F$ *against* [complex] curves at different temperature, (C) The plot of log(($F_0 - F$)/$F$) *against* log([complex]/μM) at different temperature, (D) van't Hoff plot for the interaction of BSA with this complex.

spectra position almost does not change.[1,41] During the adding of FS-DNA to Yb-complex, the absorption peak of the complex revealed reduction intensity without shift, which illustrates the existence of the groove binding between the FS-DNA and Yb-complex. Besides, to explain the complex binding affinity, its intrinsic binding constants ($K_b$) can be determined using the eqn (9):[42]

$$[Q]/(\varepsilon_a - \varepsilon_f) = [Q]/(\varepsilon_b - \varepsilon_f) + 1/K_b(\varepsilon_b - \varepsilon_f) \quad (9)$$

In the above equation, the extinction coefficient $\varepsilon_f$, $\varepsilon_b$, and $\varepsilon_a$ correspond to the extinction coefficient for the Yb-complex in a free state, the fully bound form, and $A_{obsd}$/[complex], respectively and [Q] is the FS-DNA concentration. $K_b$ was 1.49 × $10^5$ $M^{-1}$ (Fig. 5(B)), which was lower than that of the classic intercalation EtBr (1.4 × $10^6$ $M^{-1}$).[43] This result can be revealed that the interaction kind between FS-DNA and the ytterbium complex (non-intercalation) was differenced from EtBr.

### 3.3. Protein-binding

**3.3.1. The absorption titration.** The electronic absorption study is a useful method to investigate the protein structural change.[44] The absorption spectra of the aqueous BSA solution has two absorption peaks, which are referred to the framework conformation of BSA (sharp band at 212 nm) and the π → π* transition of Tyr, Phe, and Trp amino acids (weak UV-vis band at 280 nm).[45] The BSA electronic spectra (10 μM) in the absence and presence of the Yb-complex (0.5–6.5 μM) are indicated in Fig. 5(C). With the adding of the Yb-complex, the BSA absorption intensity was reduced without shifted in the $\lambda_{max}$, which is a suggestion for the binding of BSA with the Yb-complex and the interaction of this complex and BSA are non-intercalative binding modes. If the $\lambda_{max}$ was not changed at a constant BSA concentration, it means that the Yb-complex interaction reduced the protein absorption without change in the local dielectric surroundings of Tyr and Trp. Eqn (9) used for calculating of the $K_b$ ([Q] = [complex]). The $K_b$ values for ytterbium complex at 298 K was 2.13 × $10^5$ $M^{-1}$ (Fig. 5(D)). This value of

Table 2 The binding constant ($K_b$), the number of the binding sites ($n$), the biomolecular quenching rate constant $k_q$, the Stern–Volmer constant ($K_{SV}$), and thermodynamic parameters ($\Delta S^\circ$, $\Delta H^\circ$, and $\Delta G^\circ$) for the interaction of BSA with ytterbium complex at various temperatures

| | | | $K_b \times 10^{-5}$ ($M^{-1}$) | | | | | |
|---|---|---|---|---|---|---|---|---|
| $T$ (K) | $k_q \times 10^{-12}$ ($M^{-1}$ $s^{-1}$) | $K_{SV} \times 10^{-5}$ ($M^{-1}$) | UV | Fluorescence | $n$ | $\Delta S^\circ$ (J $mol^{-1}$ $K^{-1}$) | $\Delta H^\circ$ (kJ $mol^{-1}$) | $\Delta G^\circ$ (kJ $mol^{-1}$) |
| 290 | 1.51 ± 0.04 | 1.51 ± 0.04 | | 13.1 ± 0.06 | 1.17 | | | −33.97 ± 0.06 |
| 295 | 1.41 ± 0.03 | 1.41 ± 0.03 | | 7.41 ± 0.05 | 1.13 | | | −33.15 ± 0.02 |
| 298 | 1.05 ± 0.05 | 1.05 ± 0.05 | 2.13 ± 0.03 | 4.89 ± 0.05 | 1.12 | −214.93 ± 0.03 | −96.43 ± 0.05 | −32.46 ± 0.05 |
| 301 | 1.02 ± 0.04 | 1.02 ± 0.04 | | 3.38 ± 0.03 | 1.09 | | | −31.86 ± 0.04 |
| 303 | 0.96 ± 0.02 | 0.96 ± 0.02 | | 2.29 ± 0.06 | 1.07 | | | −31.09 ± 0.03 |

 

binding constant suggested that the binding of BSA with the Yb-complex is a non-intercalative interaction mode.

**3.3.2. Emission spectral studies.** The emission spectrum provides information about binding sites, binding mechanism, binding mode, binding constant, and of proteins to metal complexes.[1] The BSA solution (3.0 μM) was titrated with various amounts of the Yb-complex (0.5 to 6.0 μM). The fluorescence spectra were done at $\lambda_{ex} = 280$ nm in the range 300–450 nm (Fig. 6(A)). With the addition of Yb-complex to the BSA solution, a considerable reduction in the emission intensity was detected. The $K_{SV}$ was calculated by the Stern–Volmer equation (eqn (3)). The $K_{SV}$ values for the interaction of the BSA with Yb-complex, at various temperatures, are listed in Table 2. The linear equations at 290, 298, and 303 K are shown in Fig. 6(B) (the relevant plots at 295 and 301 K are shown in Fig. S4(A)†). This figures showed that the plots were linear, which showed that only one kind of quenching mechanism happens (either static or dynamic). From Table 2, with the increased temperatures $K_{SV}$ reduced, and the $k_q$ values were higher than $2.0 \times 10^{10}$ $M^{-1}$ $s^{-1}$ (the maximum diffuse quenching constant). It is proposed that the possible quenching process of the interaction of BSA to the Yb-complex was static. The $K_b$ values and $n$ can be determined by eqn (6).[46] The results indicated in Fig. 6(C), S4(B)† and Table 2. The finding suggests that there is a significant interaction force of the Yb-complex to BSA, and just an only interaction site would be made.

The plot of ln $K_b$ against $1/T$ allows to gaining of the thermodynamics parameters of Yb(III)-BSA complex by the eqn (7) and (8) (Fig. 6(D)). The $\Delta S^\circ$, $\Delta G^\circ$, and $\Delta H^\circ$ for the binding of BSA with ytterbium complex listed in Table 2. The negative signs of $\Delta S^\circ$ and $\Delta H^\circ$ exhibited that hydrogen bonds and van der Waals interactions play primary roles in the interaction of protein to ytterbium complex; the negative signs of $\Delta G^\circ$ showed the BSA binding procedure was spontaneous.

**3.3.3. CD spectra of BSA.** The circular dichroism study is an ideal method for observing the conformation changes of BSA.[47] As revealed in Fig. 7(A), the circular dichroism spectra of BSA reveal two negative peaks at 208 and 220 nm, which belong to $\pi \rightarrow \pi^*$ and $n \rightarrow \pi^*$ to the bond of the α-helix.[45,47] By adding of the Yb(III) complex to BSA solution, the CD signal decreased. But, the circular dichroism spectra in the absence and presence of the Yb-complex were similar in position, proposing that the BSA structure was mainly α-helical. Moreover, the α-helical content of protein and the Yb complex–protein complex can be given through eqn (10) and (11):[36]

$$\mathrm{MRE} = \frac{\text{observed CD (mdeg)}}{10 C_p n l} \quad (10)$$

$$\alpha\text{-Helix}(\%) = \frac{-(\mathrm{MRE})_{208} - 4000 \text{ CD (mdeg)}}{33000 - 4000} \times 100 \quad (11)$$

Here $MRE_{208}$ is the BSA ellipticity at 208 nm, $C_p$ is the molar concentration of protein, $l$ is the path length (1.0 cm), $n$ denotes the amino acid residues number (for BSA $n = 583$), 33 000 is the $MRE_{208}$ a pure α-helical value and 4000 is the $MRE_{208}$ of the random and β-form coil conformation cross. This data exposes that the content of α-helical for the ytterbium complex-protein

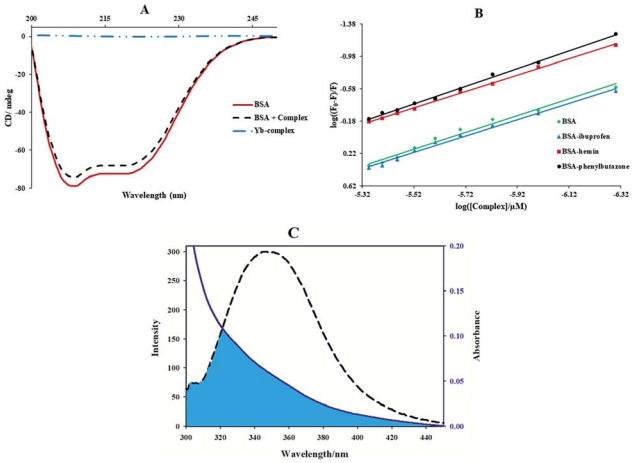


Fig. 7 (A) CD spectra of BSA solutions (0.7 μM) in the presence and absence of Yb-complex (0.7 μM); (B) effect of site marker to Yb complex–BSA system, plots of $\log((F_0 - F)/F)$ *versus* $\log([\text{complex}]/\mu M)$ in fluorescence study ([BSA] = [ibuprofen] = [phenylbutazone] = 3 μM, [hemin] = 0.3 μM, [Yb complex] = 0.5–6.0 μM and $\lambda_{ex} = 280$ nm); (C) the overlap of the emission spectrum of BSA (dashed lines) and the UV-vis spectrum (solid lines) Yb complex, [BSA] = [complex] = 3 μM.

is 48.7%, which has slightly reduced compared with the free protein (52.8%). The results reveal that BSA binds with Yb complex cause in small changes in the BSA conformation.

**3.3.4. Competitive experiments for BSA.** In BSA, there are three binding sites: site I (subdomain IIA), site II (subdomain IIIA), and site III (subdomain IB). Many ligands like phenylbutazone, azapropazone, and warfarin were applied as site marker of site I. In contrast, indoxylsulphate, diazepam, and ibuprofen were considered to bind to the site II, and hemin specially bind to site III.[48,49] The competitive study with site markers hemin, ibuprofen, and phenylbutazone were performed to recognize the particular binding site for complex on BSA, and $K_b$ values were determined by eqn (6) (Fig. 7(B)). The $K_b$ in the existence of hemin in the Yb-complex-BSA solution ($1.62 \times 10^5$ $M^{-1}$) is mainly lesser than the initial Yb-complex-BSA solution ($7.58 \times 10^5$ $M^{-1}$). But, the $K_b$ values in the existence of ibuprofen and phenylbutazone in the Yb-complex-BSA solution ($6.16 \times 10^5$ $M^{-1}$ and $4.26 \times 10^5$ $M^{-1}$, respectively) have insignificant changes. It was concluded that the Yb-complex binds to the site III of BSA.

**3.3.5. Binding distance and energy transfer.** Förster's theory was applied to evaluate molecular distances between the bound compound and the protein residues. It occurred at the molecular distance in 2–8 nm when the UV-vis band of a compound (acceptor) overlapped with the fluorescence band of protein (donor).[50] Fig. 7(C) illustrations the overlap between the fluorescence spectrum of protein and the electronic spectrum of the Yb-complex. The noticeable overlap showed that there was a direct resonance energy transfer from protein to the Yb-complex. The distance ($r$) from Trp-214 of protein to the complex and the energy transfer efficiency ($E$) were determined by eqn (12):

Table 3 The energy transfer efficiency ($E$), the overlap integral ($J$), Förster critical distance ($R_0$), and the distance to tryptophan residue of protein ($r$) in interaction of BSA with Yb complex ([Yb-complex] = [BSA] = $3 \times 10^{-6}$ M, $\lambda_{ex}$ = 280 nm and $T$ = 25 °C)

| $E$ | $J$ (cm$^3$ L mol$^{-1}$) $\times 10^{-13}$ | $R_0$ (nm) | $r$ (nm) |
|---|---|---|---|
| 0.26 | 5.37 | 2.30 | 2.69 |

$$E = 1 - \frac{F}{F_0} = \frac{{R_0}^6}{{R_0}^6 + r^6} \quad (12)$$

where $F$ and $F_0$ are the BSA emission intensities in the presence and absence of the Yb complex. $R_0$ is the critical distance when the transfer efficiency is 50%, $R_0$ were determined using eqn (13):

$$R_0{}^6 = 8.79 \times 10^{-25}\, K^2 n^{-4} \varnothing J \quad (13)$$

Here $J$ is the overlap integral of the UV-vis and the fluorescence spectrum, $\varnothing$ is the emission quantum yield of BSA, $K^2$ is the space factor of orientation, and $n$ is the medium refractive index. The eqn (14) can give $J$:

$$J = \frac{\sum F(\lambda)\varepsilon(\lambda)\lambda^4 \Delta\lambda}{\sum F(\lambda)\Delta\lambda} \quad (14)$$

Herein, $\varepsilon(\lambda)$ is the molar electronic coefficient of Yb complex at wavelength $\lambda$, and $F(\lambda)$ is the BSA fluorescence intensity. In the study conditions, $K^2 = 2/3$, $n = 1.336$ and $\varnothing = 0.15$.[51] According to experimental data of $J(\lambda)$, $R_0$, $r$, and $E$ (Table 3), the average distance between BSA and the Yb-complex falls into the 2–8 nm interval, and 0.5 $R_0 < r < 1.5$ $R_0$, therefore the transfer of energy from protein to the Yb-complex is possible.[47]

### 3.4. Docking process

**3.4.1. Docking study with DNA.** Docking study was done to investigate the ideal interaction site and best compounds conformation on the DNA with the lowest energy. The lowest binding energy and $K_i$ for the interaction of DNA with Yb-complex were obtained to be −8.28 kcal mol$^{-1}$ and 0.83 μM, respectively (Table 4). Fig. 8(A) showed that the Yb-complex placed in the DNA minor groove. The presence of non-polar fragment and polar groups in the Yb complex assist in the binding with DNA. Thus, considering the results of theoretical calculations and experimental methods, it could be concluded that the ytterbium complex interacted through grooves binding.

Table 4 The binding energies and inhibition constants of Yb-complex for the binding site of DNA and BSA

| Macromolecule | | Binding energy (kcal mol$^{-1}$) | $K_i$ (μM) |
|---|---|---|---|
| DNA | | −8.28 | 0.83 |
| BSA | Site I | −6.80 | 9.57 |
| | Site II | −7.51 | 3.29 |
| | Site III | −7.85 | 1.72 |

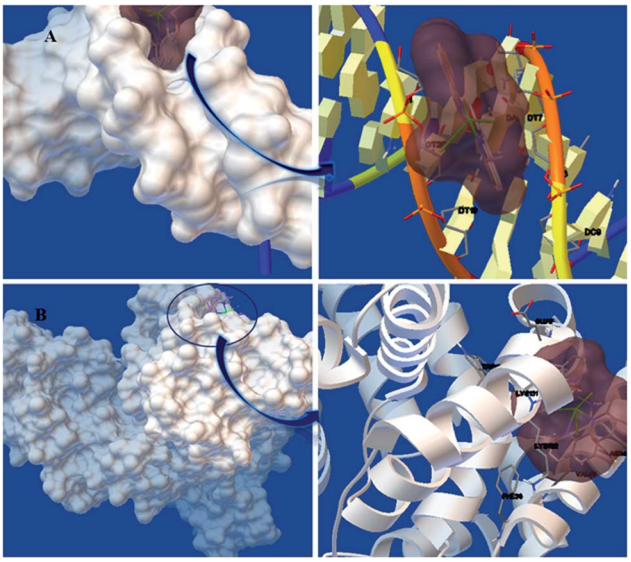


Fig. 8 The docked model of the binding between ytterbium complex and (A) DNA and (B) BSA.

**3.4.2. Docking study with BSA.** As can be seen in Table 4, site III has the lowest binding energy (−7.85 kcal mol$^{-1}$), confirming the results of the experimental techniques. According to Fig. 8(B), Yb-complex is surrounded by some amino acid residues, namely: GLU17, LYS20, PHE36, VAL40, ASN44, LYS131, LYS132, and TRP134. Some residues that interacted with the Yb complex are polar causes the complex to interact easily with BSA *via* noncovalent interactions as well as van der Waals force. The hydrogen bonding analysis in the molecular docking studies was performed and this study was observed without hydrogen bonding. Also, docking studies other sites of BSA illustrated that the Yb complex has a more binding affinity in site III (subdomain IB), where it approximately confirms the competition studies.

### 3.5. DNA cleavage experiment

Gel electrophoresis is a valued method used for purification, qualification, and separation of DNA pieces. This technique is easy to perform, simple, and able to resolve fragments of DNA that cannot be separated by other means.[48,52] The location of DNA on the agarose gel can be traced by smearing with a lower amount of EtBr. DNA cleavage experiment using FS-DNA ($1.4 \times 10^{-3}$ M) was carried out by the Yb-complex in the presence (lanes 1′–5′) and absence (lanes 1–5) of oxidant, $H_2O_2$ (20 mM, Fig. 9(A)). In lanes 1 and 1′ (control) without the Yb-complex, not any FS-DNA cleavage was detected. Lanes 2–5 and 2′–5′ indicated DNA treated with enhancing the concentration of this compound (1.2, 2.5, 3.7, and 5.0 mM). It can be seen from Fig. 9(A) that the ytterbium complex at various amounts can cleave FS-DNA. But with enhancing the concentration of the Yb-complex, due to increased cleavage of FS-DNA. Moreover, all of DNA–Yb-complex solutions show slightly decreased mobility

 

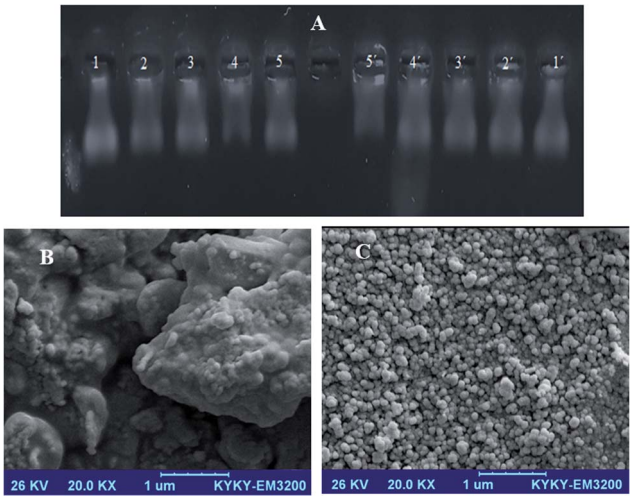


Fig. 9 (A) Gel electrophoresis diagram presentation the FS-DNA cleavage by the ytterbium complex at room temperature; lane 1: FS-DNA ($1.4 \times 10^{-3}$ M) control; lane 2: complex ($1.2 \times 10^{-3}$ M) and FS-DNA; lane 3: complex ($2.5 \times 10^{-3}$ M) and FS-DNA; lane 4: complex ($3.7 \times 10^{-3}$ M) and FS-DNA; lane 5: complex ($5.0 \times 10^{-3}$ M) and FS-DNA; and lane 1′–5′: similar concentrations of the Yb complex and DNA in the lines 1–5 in the presence of $H_2O_2$ (20 mM). (B) SEM images of the SNEP, and (C) SEM images of the LNEP.

concerning control. The DNA migration decreased with growing Yb-complex concentration (lanes 2–5 and 2′–5′). Also, the DNA cleavage efficacy is higher in the existence of the hydrogen peroxide. The photograph indicates the bands with different bandwidth (smear pattern). However, with the increasing in the Yb-complex amount, the increasing of smearing was detected for groups.[20]

### 3.6. Anticancer activity

**3.6.1. Characterization of SNEP and LNEP.** Bsae on inductively coupled plasma (ICP) assay, the amount existing of Yb in the LNEP and SNEP were determine. The encapsulation efficiency of Yb-complex in SNEP and LNEP were obtained

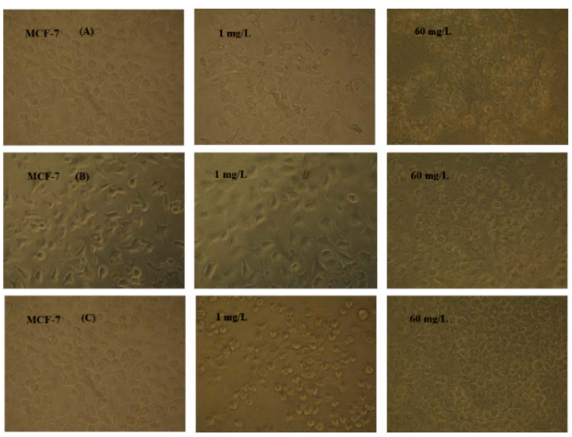


Fig. 10 Microscopic photographs of the MCF-7 cancer cells in the presence and absence of various amounts of the (A) ytterbium complex, (B) SNPE, and (C) LNPE.

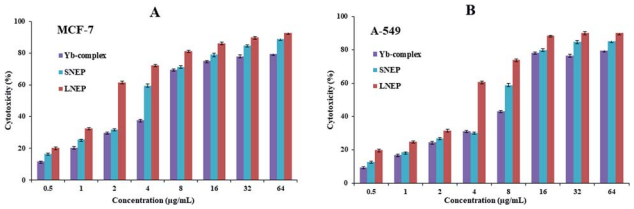


Fig. 11 Plans of cytotoxicity percentage against the ytterbium complex, SNPE, and LNPE concentrations against the A-549 and MCF-7 cell lines. Data are expressed as mean ± SD of three experiments.

11.63% and 13.04%, respectively. The SEM images of the SNEP and LNEP were indicated in Fig. 9(B and C), respectively. Also, zeta potential of the SNEP and LNEP were showed in Fig. S5.† It can be seen, the SNEP and LNEP average sizes were 50.3 and 48.6 nm, respectively. Also, the particle size of the Yb complex in LNEP was smaller than SNEP.

**3.6.2. Anticancer analyse.** The influence of the ytterbium complex, LNEP, and SNEP on the cell lines of the human lung cancer (A-549) and human breast cancer (MCF-7) was examined using the MTT test. Fig. 10 indicated the anticancer properties of the ytterbium complex, LNEP, and SNEP on MCF-7 cell lines. The results reveal that the complexes can prevent cell proliferation in a dose-dependent manner. Moreover, Fig. 11 indicated a plot of the cytotoxicity percentage against the Yb(III) complex concentration, SNEP, and LNEP. These results showed a reduction in the cancer cell number by enhancing these compound concentrations. The values of $IC_{50}$ found for the complex, SNEP, and LNEP were listed in Table 5. The maximum cell inhibition was detected at a concentration of 64 μM. These data showed that the $IC_{50}$ value found for this SNEP and LNEP was smaller than the $IC_{50}$ value of the Yb complex. Thus, the diffusion of the Yb complex into tumor cells can be simplified by the lipid and starch, and its anticancer properties can be enhanced.

### 3.7. Antibacterial and antifungal assay

Recently, it has essential for novel antibacterial and antifungal agents.[15] Different techniques tested the antimicrobial activity of the ytterbium complex against bacteria and fungi. The values of the zone of inhibition, inoculation time, MBC, and MIC were listed in Table 6.

The Yb-complex was significantly displaying properties against different bacteria and fungi, especially *C. albicans*, *A. baumannii*, *E. coli*, and MRSA. An effect of the Yb(III) complex concentration with 700 CFU of *S. typhi* illustrations in Fig. 12(A).

Table 5 $IC_{50}$ of the ytterbium complex, LNPE, and SNPE against the cell lines of A-549 and MCF-7

| | $IC_{50}$ (μg $mL^{-1}$) | | |
|---|---|---|---|
| Cell lines | Yb-complex | LNEP | SENP |
| A-549 | 10.2 | 3.29 | 6.80 |
| MCF-7 | 5.75 | 1.62 | 3.36 |

Table 6 The antibacterial and antifungal activities of ytterbium complex by the zone of inhibition (mm), minimum inhibitory concentrations (MIC, μg $mL^{-1}$), minimum bactericidal concentrations (MBC, mg $mL^{-1}$) and inoculation time (*h*) against fungi and bacteria

| Bacteria type | Bacteria or fungi | Zone of inhibition (mm) | MIC (μg $mL^{-1}$) | MBC (mg $mL^{-1}$) | Inoculation time (*h*) |
|---|---|---|---|---|---|
| Fungi | *C. albicans* | 55 | 62 | 1.0 | 24 |
| Gram-negative | *S. typhi* | 32 | 62 | 2.0 | 48 |
| | *P. aeruginosa* | 21 | 125 | 4.0 | 48 |
| | *A. baumannii* | 45 | 31 | 2.0 | 48 |
| | *K. pneumoniae* | 33 | 62 | 0.5 | 24 |
| | *E. coli* | 38 | 31 | 2.0 | 24 |
| Gram-positive | MRSA | 34 | 125 | 4.0 | 48 |
| | VRE | 9 | 31 | 2.0 | 48 |
| | *E. faecalis* | 8 | 125 | 4.0 | 48 |
| | *E. faecium* | 21 | 125 | 4.0 | 48 |

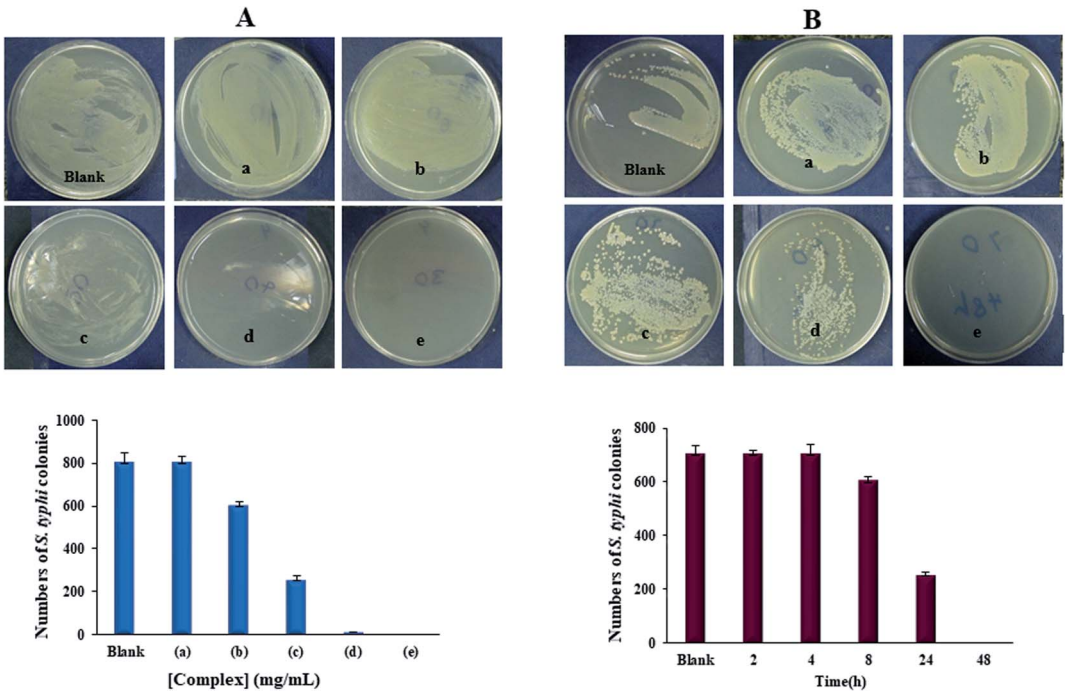


Fig. 12 The amount raise of bacterial colonies as an effect of (A) the Yb complex concentration with 800 CFU of *S. typhi*. Inset is MH plate photographs raised under the condition (a) 0.25, (b) 0.5, (c) 1.0, (d) 2.0 and (e) 4.0 mg $mL^{-1}$, (B) the inoculation time of ytterbium complex with 700 CFU of *S. typhi*. Inset is MH plate photographs incubated: (a) 2 h, (b) 4 h, (c) 8 h, (d) 24 h, and (e) 48 h. Data are expressed as mean ± SD of three experiments.

The substantial decrease in the extent of bacterial colonies was observed in 2.0 mg of Yb-complex, showing antimicrobial properties by growing the Yb-complex concentrations. MH standard with 5 mg $mL^{-1}$ of Yb-complex and 700 CFU of *S. typhi* supplemented for various time distances. Fig. 12(B) and Table 6 indicated that the *S. typhi* colonies were killed entirely after 48 hours of inoculation, and the calculation of bacteria decrease was nearly 100% after 4–48 hours of injection. The data revealed that this complex has produced the marked enhancement in the potency as antifungal and antibacterial agents. Such increased activity of Yb(III) complex can be explained on the basis of chelation theory. Chelation considerably decreases the polarity of the metal ion, which further leads to the enhancement of the lipophilicity of the complex. Since the microorganism cell is surrounded by a lipid membrane which favors the passage of only the lipid soluble materials, increased lipophilicities allows the penetration of complex into lipid membranes and blocking of the metal binding sites in the enzymes of the microorganisms. Also, the antibacterial mechanism was hypothesized that ytterbium(III) complex has an effect on the pathogenic bacteria cell proliferation.[15,53,54]

## 4. Conclusion

In this research, the biology application of the ytterbium-complex was investigated. The FS-DNA and BSA interaction properties of the Yb complex were comprehensively investigated by various techniques, containing UV-vis spectroscopy,

 

emission spectra, competitive experiments, CD spectroscopy, and molecular docking calculations. The results showed the excellent binding affinity of the Yb-complex to FS-DNA and BSA; besides the emission quenching of FS-DNA and BSA resulted from the combined static-dynamic and static process, respectively. Moreover, groove binding (hydrophobic interaction and van der Waals force for DNA and BSA, respectively) played major roles in stabilizing the Yb-complex with DNA/BSA. From molecular docking and competitive binding studies, it exhibited that site 3 of BSA is the binding site of interaction Yb-complex to BSA. The agreement of molecular docking and experimental results can be given as powerful support for the validity of docking studies. Moreover, the Yb complex successfully cleaved DNA in the absence and presence of hydrogen peroxide and has high antimicrobial activity on several bacterial and fungi. In addition, the drug carrier forms of the Yb complex (SNEP and LNEP) were prepared. These complexes exhibited significant antitumor properties against cell lines of A-549 and MCF-7. Briefly, it can be seen that ytterbium complex bonds in the groove of FS-DNA as well as can be transported professionally through BSA in the blood. Also, this complex has been obtained to revelation antitumor, antibacterial, and antifungal activities. Therefore, the foundation knowledge from this work would be helpful for the improvement of novel therapeutic reagents for diseases.

## Conflicts of interest

The authors declare that they have no known competing financial interests or personal relationships that could have appeared to influence the work reported in this paper.

## Acknowledgements

The financial supports of Research Councils of University of Sistan and Baluchestan are gratefully acknowledged. K. K. acknowledges financial support from the Canada Research Chairs Tier-2 award for "Bioelectrochemistry of Proteins" (Project no. 950-231116), Ontario Ministry of Research and Innovation (Project no. 35272), Discovery Grant (Project no. 3655) from Natural Sciences and Engineering Research Council of Canada (NSERC), and Canada Foundation for Innovation (Project no. 35272).

## References

1 D. Anu, P. Naveen, B. VijayaPandiyan, C. S. Frampton and M. Kaveri, An unexpected mixed valence tetranuclear copper(I/II) complex: Synthesis, structural characterization, DNA/protein binding, antioxidant and anticancer properties, *Polyhedron*, 2019, **167**, 137–150.

2 M. Anjomshoa, S. J. Fatemi, M. Torkzadeh-Mahani and H. Hadadzadeh, DNA- and BSA-binding studies and anticancer activity against human breast cancer cells (MCF-7) of the zinc(II) complex coordinated by 5,6-diphenyl-3-(2-pyridyl)-1,2,4-triazine, *Spectrochim. Acta, Part A*, 2014, **127**, 511–520, DOI: 10.1016/j.saa.2014.02.048.

3 T.-T. Zhao, X. Lu, X.-H. Yang, L.-M. Wang, X. Li, Z.-C. Wang, H.-B. Gong and H.-L. Zhu, Synthesis, biological evaluation, and molecular docking studies of 2,6-dinitro-4-(trifluoromethyl) phenoxysalicylaldoxime derivatives as novel antitubulin agents, *Bioorg. Med. Chem.*, 2012, **20**(10), 3233–3241.

4 M. Mohamadi, A. Hassankhani, S. Y. Ebrahimipour and M. Torkzadeh-Mahani, In vitro and in silico studies of the interaction of three tetrazoloquinazoline derivatives with DNA and BSA and their cytotoxicity activities against MCF-7, HT-29 and DPSC cell lines, *Int. J. Biol. Macromol.*, 2017, **94**, 85–95, DOI: 10.1016/j.ijbiomac.2016.09.113.

5 M. Sedighipoor, A. H. Kianfar, G. Mohammadnezhad, H. Görls, W. Plass, A. A. Momtazi-Borojeni and E. Abdollahi, Synthesis, crystal structure of novel unsymmetrical heterocyclic Schiff base Ni(II)/V(IV) complexes: Investigation of DNA binding, protein binding and in vitro cytotoxic activity, *Inorg. Chim. Acta*, 2019, **488**, 182–194.

6 T. Kondori, O. Shahraki, N. Akbarzadeh-T and Z. Arameesh-Boroujeni, Two Novel Bipyridine-based Cobalt(II) Complexes: Synthesis, Characterization, Molecular Docking, DNA-Binding and Biological Evaluation, *J. Biomol. Struct. Dyn.*, 2020, 1–27, DOI: 10.1080/07391102.2020.1713893.

7 B.-L. Wang, D.-Q. Pan, K.-L. Zhou, Y.-Y. Lou and J.-H. Shi, Multi-spectroscopic approaches and molecular simulation research of the intermolecular interaction between the angiotensin-converting enzyme inhibitor (ACE inhibitor) benazepril and bovine serum albumin (BSA), *Spectrochim. Acta, Part A*, 2019, **212**, 15–24.

8 J.-h. Shi, D.-q. Pan, M. Jiang, T.-T. Liu and Q. Wang, In vitro study on binding interaction of quinapril with bovine serum albumin (BSA) using multi-spectroscopic and molecular docking methods, *J. Biomol. Struct. Dyn.*, 2017, **35**(10), 2211–2223.

9 J.-H. Shi, Y.-Y. Lou, K.-L. Zhou and D.-Q. Pan, Elucidation of intermolecular interaction of bovine serum albumin with Fenhexamid: a biophysical prospect, *J. Photochem. Photobiol., B*, 2018, **180**, 125–133.

10 A. R. Timerbaev, C. G. Hartinger, S. S. Aleksenko and B. K. Keppler, Interactions of antitumor metallodrugs with serum proteins: advances in characterization using modern analytical methodology, *Chem. Rev.*, 2006, **106**(6), 2224–2248.

11 X.-Q. Song, Z.-G. Wang, Y. Wang, Y.-Y. Huang, Y.-X. Sun, Y. Ouyang, C.-Z. Xie and J.-Y. Xu, Syntheses, characterization, DNA/HSA binding ability and antitumor activities of a family of isostructural binuclear lanthanide complexes containing hydrazine Schiff base, *J. Biomol. Struct. Dyn.*, 2020, **38**(3), 733–743, DOI: 10.1080/07391102.2019.1587511.

12 S. Niroomand, M. Khorasani-Motlagh, M. Noroozifar, S. Jahani and A. Moodi, Photochemical and DFT studies on DNA-binding ability and antibacterial activity of lanthanum(III)-phenanthroline complex, *J. Mol. Struct.*, 2017, **1130**, 940–950.

13 A.-C. Munteanu, M. Badea, R. Olar, L. Silvestro, C. Dulea, C.-D. Negut and V. Uivarosi, Synthesis and structural investigation of new bio-relevant complexes of lanthanides with 5-hydroxyflavone: DNA binding and protein interaction studies, *Molecules*, 2016, **21**(12), 1737.

14 S. Jahani, M. Noroozifar, M. Khorasani-Motlagh, M. Torkzadeh-Mahani and M. Adeli-Sardou, In vitro cytotoxicity studies of parent and nanoencapsulated holmium-2,9-dimethyl-1,10-phenanthroline complex toward fish-salmon DNA-binding properties and antibacterial activity, *J. Biomol. Struct. Dyn.*, 2019, **37**(17), 4437–4449, DOI: 10.1080/07391102.2018.1557077.

15 B. H. Hussein, H. A. Azab, M. F. El-Azab and A. I. El-Falouji, A novel anti-tumor agent, Ln(III) 2-thioacetate benzothiazole induces anti-angiogenic effect and cell death in cancer cell lines, *Eur. J. Med. Chem.*, 2012, **51**, 99–109.

16 J.-H. Wei, Z.-F. Chen, J.-L. Qin, Y.-C. Liu, Z.-Q. Li, T.-M. Khan, M. Wang, Y.-H. Jiang, W.-Y. Shen and H. Liang, Water-soluble oxoglaucine-Y(III), Dy(III) complexes: in vitro and in vivo anticancer activities by triggering DNA damage, leading to S phase arrest and apoptosis, *Dalton Trans.*, 2015, **44**(25), 11408–11419.

17 K. Andiappan, A. Sanmugam, E. Deivanayagam, K. Karuppasamy, H.-S. Kim and D. Vikraman, In vitro cytotoxicity activity of novel Schiff base ligand–lanthanide complexes, *Sci. Rep.*, 2018, **8**(1), 3054.

18 S. Akhavan, E. Assadpour, I. Katouzian and S. M. Jafari, Lipid nano scale cargos for the protection and delivery of food bioactive ingredients and nutraceuticals, *Trends Food Sci. Technol.*, 2018, **74**, 132–146.

19 S. Dianat, A. Bordbar, S. Tangestaninejad, B. Yadollahi, S. Zarkesh-Esfahani and P. Habibi, In vitro antitumor activity of parent and nano-encapsulated mono cobalt-substituted Keggin polyoxotungstate and its ctDNA binding properties, *Chem.-Biol. Interact.*, 2014, **215**, 25–32.

20 Z. Aramesh-Boroujeni, M. Khorasani-Motlagh and M. Noroozifar, Multispectroscopic DNA-binding studies of a terbium(III) complex containing 2,2′-bipyridine ligand, *J. Biomol. Struct. Dyn.*, 2016, **34**(2), 414–426.

21 Z. Aramesh-Boroujeni, A.-K. Bordbar, M. Khorasani-Motlagh, N. Fani, E. Sattarinezhad and M. Noroozifar, Computational and experimental study on the interaction of three novel rare earth complexes containing 2,9-dimethyl-1,10-phenanthroline with human serum albumin, *J. Iran. Chem. Soc.*, 2018, **15**(7), 1581–1591, DOI: 10.1007/s13738-018-1356-5.

22 Z. Aramesh-Boroujeni, A.-K. Bordbar, M. Khorasani-Motlagh, E. Sattarinezhad, N. Fani and M. Noroozifar, Synthesis, characterization, and binding assessment with human serum albumin of three bipyridine lanthanide(III) complexes, *J. Biomol. Struct. Dyn.*, 2019, **37**(6), 1438–1450, DOI: 10.1080/07391102.2018.1464959.

23 Z. Aramesh-Boroujeni, S. Jahani, M. Khorasani-Motlagh, K. Kerman, N. Aramesh, S. Asadpour and M. Noroozifar, Experimental and theoretical investigations of Dy(III) complex with 2,2′-bipyridine ligand: DNA and BSA interactions and antimicrobial activity study, *J. Biomol. Struct. Dyn.*, 2019, 1–18, DOI: 10.1080/07391102.2019.1689170.

24 Z. Aramesh-Boroujeni, S. Jahani, M. Khorasani-Motlagh, K. Kerman and M. Noroozifar, Evaluation of DNA, BSA binding, DNA cleavage and antimicrobial activity of ytterbium(III) complex containing 2,2'-bipyridine ligand, *J. Biomol. Struct. Dyn.*, 2020, **38**(6), 1711–1725, DOI: 10.1080/07391102.2019.1617788.

25 Z. Aramesh-Boroujeni, S. Jahani, M. Khorasani-Motlagh, K. Kerman and M. Noroozifar, Evaluation of parent and nano-encapsulated terbium(III) complex toward its photoluminescence properties, FS-DNA, BSA binding affinity, and biological applications, *J. Trace Elem. Med. Biol.*, 2020, **61**, 126564, DOI: 10.1016/j.jtemb.2020.126564.

26 H.-J. Yu, S.-M. Huang, L.-Y. Li, H.-N. Jia, H. Chao, Z.-W. Mao, J.-Z. Liu and L.-N. Ji, Synthesis, DNA-binding and photocleavage studies of ruthenium complexes $[Ru(bpy)_2(mitatp)]^{2+}$ and $[Ru(bpy)_2(nitatp)]^{2+}$, *J. Inorg. Biochem.*, 2009, **103**(6), 881–890, DOI: 10.1016/j.jinorgbio.2009.03.005.

27 J.-H. Shi, Q. Wang, D.-Q. Pan, T.-T. Liu and M. Jiang, Characterization of interactions of simvastatin, pravastatin, fluvastatin, and pitavastatin with bovine serum albumin: multiple spectroscopic and molecular docking, *J. Biomol. Struct. Dyn.*, 2017, **35**(7), 1529–1546.

28 F. Neese, The ORCA program system, *Wiley Interdiscip. Rev.: Comput. Mol. Sci.*, 2012, **2**(1), 73–78.

29 G. M. Morris, D. S. Goodsell, R. S. Halliday, R. Huey, W. E. Hart, R. K. Belew and A. J. Olson, Automated docking using a Lamarckian genetic algorithm and an empirical binding free energy function, *J. Comput. Chem.*, 1998, **19**(14), 1639–1662.

30 Y. Yu, Y. Huang, L. Zhang, Z. Lin and G. Wang, Growth and Spectral Assessment of $Yb^{3+}$-Doped $KBaGd(MoO_4)_3$ Crystal: A Candidate for Ultrashort Pulse and Tunable Lasers, *PLoS ONE*, 2013, **8**, e54450.

31 X. M. Ferré, *Crystal growth, optical characterisation and laser operation of $Yb^{3+}$ in monoclinic double tungstates*, Rovira i Virgili University, 2004.

32 D. He, L. Wang, L. Wang, X. Li and Y. Xu, Spectroscopic studies on the interactions between novel bisnaphthalimide derivatives and calf thymus DNA, *J. Photochem. Photobiol., B*, 2017, **166**, 333–340, DOI: 10.1016/j.jphotobiol.2016.12.003.

33 N. Shahabadi, M. Hakimi, T. Morovati, M. Falsafi and S. M. Fili, Experimental and molecular modeling studies on the DNA-binding of diazacyclam-based acrocyclic copper complex, *J. Photochem. Photobiol., B*, 2017, **167**, 7–14.

34 E. Moradinia, M. Mansournia, Z. Aramesh-Boroujeni and A. K. Bordbar, New transition metal complexes of 9,10-phenanthrenequinone p-toluyl hydrazone Schiff base: Synthesis, spectroscopy, DNA and HSA interactions, antimicrobial, DFT and docking studies, *Appl. Organomet. Chem.*, 2019, **33**(5), e4893, DOI: 10.1002/aoc.4893.

35 J. R. Lakowicz and G. Weber, Quenching of fluorescence by oxygen. Probe for structural fluctuations in macromolecules, *Biochemistry*, 1973, **12**(21), 4161–4170.

36 Q. Wang, C.-r. Huang, M. Jiang, Y.-y. Zhu, J. Wang, J. Chen and J.-h. Shi, Binding interaction of atorvastatin with bovine serum albumin: Spectroscopic methods and molecular docking, *Spectrochim. Acta, Part A*, 2016, **156**, 155–163.

37 J.-H. Shi, Y.-Y. Lou, K.-L. Zhou and D.-Q. Pan, Exploration of intermolecular interaction of calf thymus DNA with sulfosulfuron using multi-spectroscopic and molecular docking techniques, *Spectrochim. Acta, Part A*, 2018, **204**, 209–216.

38 X.-M. Dong, Y.-Y. Lou, K.-L. Zhou and J.-H. Shi, Exploration of association of telmisartan with calf thymus DNA using a series of spectroscopic methodologies and theoretical calculation, *J. Mol. Liq.*, 2018, **266**, 1–9.

39 F. Jalali and P. S. Dorraji, Interaction of anthelmintic drug (thiabendazole) with DNA: Spectroscopic and molecular modeling studies, *Arabian J. Chem.*, 2017, **10**, S3947–S3954, DOI: 10.1016/j.arabjc.2014.06.001.

40 A. Mukherjee, S. Mondal and B. Singh, Spectroscopic, electrochemical and molecular docking study of the binding interaction of a small molecule 5H-naptho[2,1-f][1,2]oxathieaphine 2,2-dioxide with calf thymus DNA, *Int. J. Biol. Macromol.*, 2017, **101**, 527–535.

41 S. Yadav, I. Yousuf, M. Usman, M. Ahmad, F. Arjmand and S. Tabassum, Synthesis and spectroscopic characterization of diorganotin(IV) complexes of N′-(4-hydroxypent-3-en-2-ylidene) isonicotinohydrazide: chemotherapeutic potential validation by in vitro interaction studies with DNA/HSA, DFT, molecular docking and cytotoxic activity, *RSC Adv.*, 2015, **5**(63), 50673–50690.

42 A. Haque, I. Khan, S. I. Hassan and M. S. Khan, Interaction studies of cholinium-based ionic liquids with calf thymus DNA: spectrophotometric and computational methods, *J. Mol. Liq.*, 2017, **237**, 201–207.

43 U. Chaveerach, A. Meenongwa, Y. Trongpanich, C. Soikum and P. Chaveerach, DNA binding and cleavage behaviors of copper(II) complexes with amidino-O-methylurea and N-methylphenyl-amidino-O-methylurea, and their antibacterial activities, *Polyhedron*, 2010, **29**(2), 731–738, DOI: 10.1016/j.poly.2009.10.031.

44 X.-W. Li, X.-H. Zhao, Y.-T. Li and Z.-Y. Wu, Synthesis and crystal structure of bicopper(II) complexes: The influence of bridging ligands on DNA/BSA binding behaviors and in vitro antitumor activity, *Inorg. Chim. Acta*, 2019, **488**, 219–228.

45 G.-F. Shen, T.-T. Liu, Q. Wang, M. Jiang and J.-H. Shi, Spectroscopic and molecular docking studies of binding interaction of gefitinib, lapatinib and sunitinib with bovine serum albumin (BSA), *J. Photochem. Photobiol., B*, 2015, **153**, 380–390.

46 J. B. Xiao, J. W. Chen, H. Cao, F. L. Ren, C. S. Yang, Y. Chen and M. Xu, Study of the interaction between baicalin and bovine serum albumin by multi-spectroscopic method, *J. Photochem. Photobiol., A*, 2007, **191**(2–3), 222–227.

47 X.-B. Fu, Z.-H. Lin, H.-F. Liu and X.-Y. Le, A new ternary copper(II) complex derived from 2-(2′-pyridyl) benzimidazole and glycylglycine: Synthesis, characterization, DNA binding and cleavage, antioxidation and HSA interaction, *Spectrochim. Acta, Part A*, 2014, **122**, 22–33.

48 U. Katrahalli, B. C. Yallur, D. H. Manjunatha and P. M. Krishna, BSA interaction and DNA cleavage studies of anti-bacterial benzothiazol-2-yl-malonaldehyde, *J. Mol. Struct.*, 2019, **1196**, 96–104.

49 Y.-Y. Lou, K.-L. Zhou, D.-Q. Pan, J.-L. Shen and J.-H. Shi, Spectroscopic and molecular docking approaches for investigating conformation and binding characteristics of clonazepam with bovine serum albumin (BSA), *J. Photochem. Photobiol., B*, 2017, **167**, 158–167.

50 L. Zarei, Z. Asadi, M. Dusek and V. Eigner, Homodinuclear Ni(II) and Cu(II) Schiff base complexes derived from O-vanillin with a pyrazole bridge: Preparation, crystal structures, DNA and protein (BSA) binding, DNA cleavage, molecular docking and cytotoxicity study, *J. Photochem. Photobiol., A*, 2019, **374**, 145–160.

51 A. T. Buddanavar and S. T. Nandibewoor, Multi-spectroscopic characterization of bovine serum albumin upon interaction with atomoxetine, *J. Pharm. Anal*, 2017, **7**(3), 148–155.

52 S. Budagumpi, N. V. Kulkarni, G. S. Kurdekar, M. Sathisha and V. K. Revankar, Synthesis and spectroscopy of CoII, NiII, CuII and ZnII complexes derived from 3,5-disubstituted-1H-pyrazole derivative: a special emphasis on DNA binding and cleavage studies, *Eur. J. Med. Chem.*, 2010, **45**(2), 455–462.

53 K. B. Gudasi, V. C. Havanur, S. A. Patil and B. R. Patil, Antimicrobial study of newly synthesized lanthanide(III) complexes of 2-[2-hydroxy-3-methoxyphenyl]-3-[2-hydroxy-3-methoxybenzylamino]-1,2-dihydroquinazolin-4 (3H)-one) complexes of 2-[2-hydroxy-3-methoxyphenyl]-3-[2-hydroxy-3-methoxybenzylamino]-1,2-dihydroquinazolin-4 (3H)-one, *Met.-Based Drugs*, 2007, **2007**, 037348–037355.

54 D. Yinhua, M. M. Foroughi, Z. Aramesh-Boroujeni, S. Jahani, M. Peydayesh, F. Borhani, M. Khatami, M. Rohani, M. Dušek and V. Eigner, Synthesis, characterization, DNA/BSA/HSA interactions, molecular modeling, antibacterial and in vitro cytotoxic activities of a novel parent and niosome nano-encapsulated Ho(III) complex, *RSC Adv.*, 2020, DOI: 10.1039/d0ra03436c.